Oxygen holes and hybridization in the bismuthates

Arash Khazraie,* Kateryna Foyevtsova, Ilya Elfimov, and George A. Sawatzky
Department of Physics & Astronomy, University of British Columbia, Vancouver, British Columbia, Canada V6T 1Z1
and Stewart Blusson Quantum Matter Institute, University of British Columbia, Vancouver, British Columbia, Canada V6T 1Z4

(Received 8 November 2017; revised manuscript received 22 January 2018; published 2 February 2018)

Motivated by the recently renewed interest in the superconducting bismuth perovskites, we investigate the electronic structure of the parent compounds $A\mathrm{BiO_3}$ (A = Sr, Ba) using *ab initio* methods and tight-binding (TB) modeling. We use the density functional theory (DFT) in the local density approximation (LDA) to understand the role of various interactions in shaping the $A\mathrm{BiO_3}$ band structure near the Fermi level. It is established that interatomic hybridization involving Bi-6s and O-2p orbitals plays the most important role. Based on our DFT calculations, we derive a minimal TB model and demonstrate that it can describe the properties of the band structure as a function of lattice distortions, such as the opening of a charge gap with the onset of the breathing distortion and the associated condensation of holes onto a_{1g}-symmetric molecular orbitals formed by the O-2p_σ orbitals on collapsed octahedra. We also derive a single band model involving the hopping of an extended molecular orbital involving both Bi-6s and a linear combination of six O-2p orbitals which provides a very good description of the dispersion and band gaps of the low energy scale bands straddling the chemical potential.

DOI: 10.1103/PhysRevB.97.075103

I. INTRODUCTION

Hole-doped bismuth perovskites $A\mathrm{BiO_3}$ (A = Sr, Ba) have recently attracted a lot of attention as one of the few examples of transition-metal-free high-transition-temperature oxide superconductors [1–3]. The parent compounds are no less interesting, demonstrating a variety of temperature-driven electronic and structural phase transitions [4,5]. At low temperature, $\mathrm{BaBiO_3}$ and $\mathrm{SrBiO_3}$ are insulators with some characteristic distortions from an ideal cubic perovskite crystal structure. Namely, oxygen octahedra around the Bi ions exhibit alternating breathing-in and breathing-out distortions along the three cubic crystallographic directions, resulting in disproportionated Bi-O bond lengths. Additionally, the $\mathrm{O_6}$ octahedra are tilted and rotated, following a $a^-a^-c^0$ pattern in $\mathrm{BaBiO_3}$ and a $a^-a^-c^+$ pattern in $\mathrm{SrBiO_3}$ in Glazer's classification [6,7].

The insulating state of $A\mathrm{BiO_3}$ is often interpreted in terms of a charge-disproportionation model [4,5,8,9]. In this model, Bi ions with the nominal valency of 4+ disproportionate into $\mathrm{Bi^{3+}}$ and $\mathrm{Bi^{5+}}$ as $\mathrm{Ba_2^{2+}Bi^{3+}Bi^{5+}O_6^{2-}}$, which produces shorter $\mathrm{Bi^{5+}}$-O bonds and longer $\mathrm{Bi^{3+}}$-O bonds and corresponds to the valence electron occupation changing from $6s^16s^1$ to $6s^06s^2$ for the two Bi sites. This scenario, however, is not consistent with the on-site repulsion effects, the high binding energy of the Bi-6s states as observed in Refs. [10] and [11], or the strongly covalent nature of the Bi-O bonding [10–12] and is not supported by spectroscopic measurements finding little difference in the Bi valence shell occupations [13–15].

Thanks to the weakly correlated nature of the Bi-6s and O-2p electrons in $A\mathrm{BiO_3}$ [16], an accurate theoretical description of these systems is already possible in the framework of the density functional theory (DFT) and local density approximation (LDA), although a more advanced treatment of exchange and correlation effects has been shown to result in an enhancement of the gap and the electron-phonon coupling. The states bridging the Fermi energy are basically unchanged as compared to conventional DFT, indicating that the use of LDA+U or hybrid functionals merely increases the gap value [17–22]. Previous DFT studies [12,23–25] generally find that the Bi-6s states lie deeper in energy by several electron volts than the O-2p states, questioning further the charge-disproportionation model. In Ref. [25], we used DFT methods to validate an alternative microscopic model for the insulating state of $A\mathrm{BiO_3}$, considered initially by Ignatov [26], in which the hole pairs condense spatially onto collapsed $\mathrm{O_6}$ octahedra occupying molecular orbitals of the a_{1g} symmetry while all the Bi ions are close to being $6s^2$, i.e., the following process is taking place:

$$2\mathrm{Bi^{3+}}\underline{L} \rightarrow \mathrm{Bi^{3+}}\underline{L}^2 + \mathrm{Bi^{3+}},$$

where $\underline{L}$ represents a ligand hole in an a_{1g}-symmetric molecular orbital on a collapsed $\mathrm{O_6}$ octahedron. Note that in this scenario all oxygens remain equivalent in terms of charge and the resulting insulating state should be named "bond-disproportionated" rather than "charge-disproportionated."

In the present followup paper, we intend to better understand the relevance of various interactions in determining the electronic structure of $A\mathrm{BiO_3}$ and derive its minimal tight-binding (TB) model. Such a minimal model describing the low energy scale states is especially useful in constructing model Hamiltonians including the electron-phonon interactions to discuss aspects such as bipolaron formation and superconductivity in hole or electron doped systems. We first use DFT calculations to study the hybridization strengths between the constituent elements of $A\mathrm{BiO_3}$, demonstrating the extreme

*akhazr@phas.ubc.ca

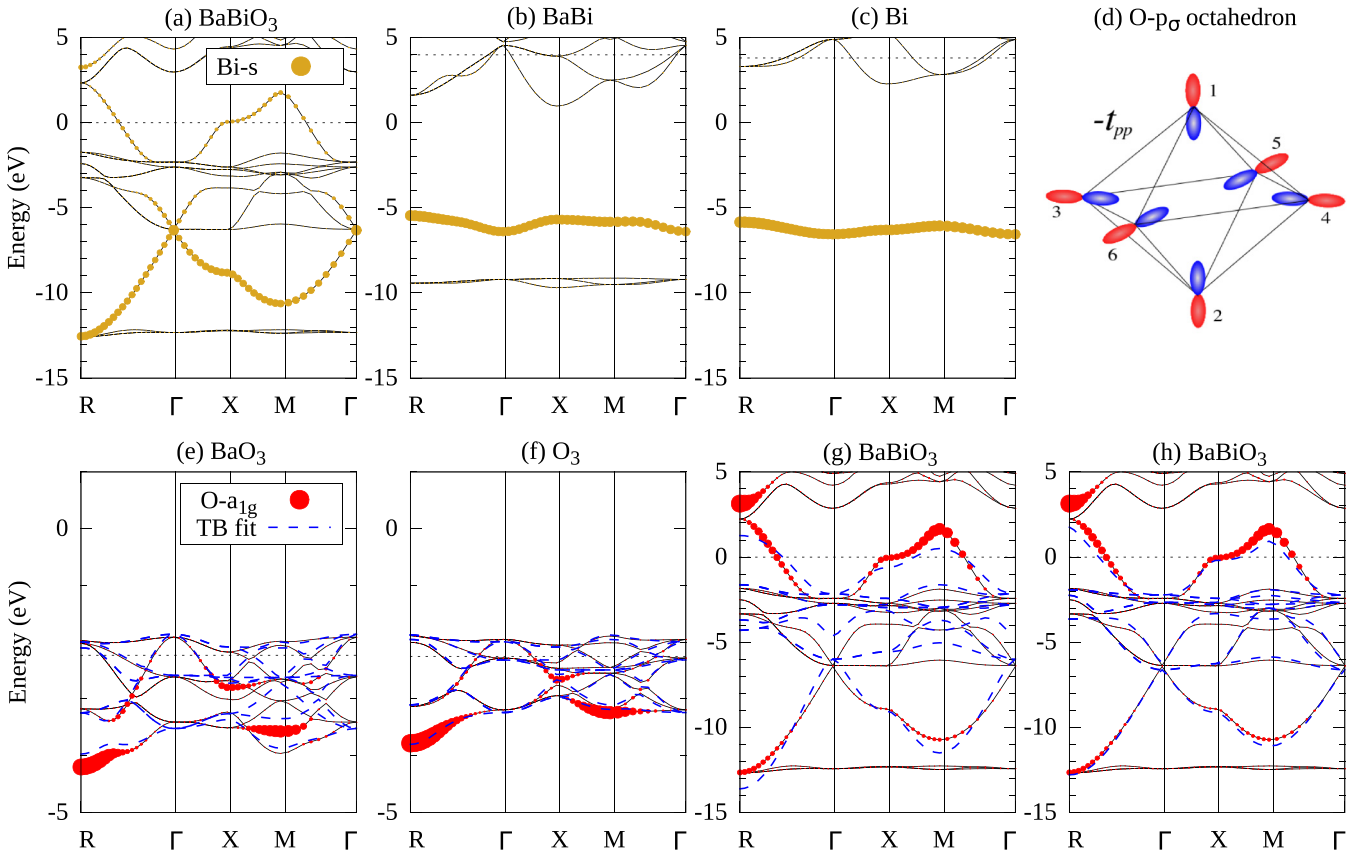

FIG. 1. The DFT (LDA) band structures of (a), (g), (h) $BaBiO_3$ and its (b) BaBi, (c) Bi, (e) BaO_3, and (f) O_3 sublattices. In (a)–(c), the yellow-colored fat bands represent the contribution of the Bi-s orbital, while in (e)–(h), the red-colored fat bands represent the contribution of the O-a_{1g} molecular orbital. The Fermi level is marked with a horizontal dashed black line. Panel (d) shows the O-a_{1g} molecular orbital combination of oxygen-p_σ orbitals in an octahedron. The oxygen sites 1 to 6 are coupled via hopping integrals $-t_{pp} = (-t_{pp\sigma} + t_{pp\pi})/2$. A nearest neighbor TB model fit of (e) BaO_3 (f) O_3, and (g)–(h) $BaBiO_3$ is shown with dashed lines. In (h), Bi-6p orbitals are added in an extended tight-binding model (ETB) for an improved fit. The parameter values resulting from the fits are listed in Table II.

effects of interatomic hybridization involving the Bi-6s and O-2p orbitals. Having determined the most relevant atomic orbitals and interactions, we then study the properties of our derived TB model as a function of structural distortions in two and three dimensions. Finally, we explore possible simplifications of the TB model with a focus on describing low-energy electronic excitations.

II. RESULTS AND DISCUSSION

A. Bi, BaBi, O_3, and BaO_3 sublattices of $BaBiO_3$

In order to study the hybridization strengths between the constituent elements of $ABiO_3$, we calculate and compare the electronic band structures of $BaBiO_3$ and of its Bi, BaBi, O_3, and BaO_3 sublattices. It is to be expected that all the conclusions in this section will be equally applicable to $SrBiO_3$ because of its close similarity to $BaBiO_3$.

The electronic structure calculations are performed with the full-potential linearized-augmented-plane-wave code WIEN2K [27]. Exchange and correlation effects are treated within the generalized gradient density approximation (GGA) [28]. For now, we will neglect the effects of lattice distortions and consider an idealized cubic unit cell containing one formula unit. A value of 4.34 Å is used for the lattice constant, taken as the average over the nearest-neighbor Bi-Bi distances in the experimentally measured distorted structure [4], and a $7 \times 7 \times 7k$-point grid is used for the Brillouin-zone integration.

As discussed earlier [12,25], the band structure of $BaBiO_3$ near the Fermi level is featured by a collection of strongly dispersive states with predominant Bi-6s and O-2p orbital characters. Most of the Bi-6s character is concentrated in the 8 eV broad lowest band centered at -10 eV [Fig. 1(a)]. In contrast, in either the BaBi [Fig. 1(b)] or the Bi [Fig. 1(c)] sublattices, the Bi-6s band width is less than 1 eV. This indicates that interatomic hopping integrals involving only Ba and Bi atomic orbitals are rather small.

Let us now consider the electronic band structures of the BaO_3 and O_3 sublattices, shown in Figs. 1(e) and 1(f), respectively. As we demonstrated in Ref. [25], it is helpful to analyze the dispersion of the O-2p states in a perovskite structure in terms of molecular orbital combinations of the O-2p_σ atomic orbitals in an isolated octahedron. There are six such combinations listed in Table I with the oxygen sites indexed in Fig. 1(d). For future reference, Table I also contains molecular orbital combinations of the O-2p_σ orbitals in an isolated square plaquette. The O-a_{1g}-symmetric molecular orbital combination is of particular interest as it is the only

TABLE I. The eigenstates and eigenvalues of an octahedron and a square plaquette of O-p_σ orbitals coupled via nearest-neighbor hopping integrals $-t_{pp} = (-t_{pp\sigma} + t_{pp\pi})/2$. For oxygen site indexing and relative orbital phases, refer to Fig. 1(d). Here, the O-p_σ orbitals' on-site energies are set to zero.

	Octahedron						Square plaquette			
O site	a_{1g}	t_{1u}	t_{1u}	t_{1u}	e_g	e_g	a_{1g}	e_u	e_u	b_{1g}
1	$\frac{1}{\sqrt{6}}$	$\frac{1}{\sqrt{2}}$	0	0	$\frac{1}{\sqrt{3}}$	0	$\frac{1}{\sqrt{4}}$	$\frac{1}{\sqrt{2}}$	0	$\frac{1}{\sqrt{4}}$
2	$\frac{1}{\sqrt{6}}$	$\frac{-1}{\sqrt{2}}$	0	0	$\frac{1}{\sqrt{3}}$	0	$\frac{1}{\sqrt{4}}$	$\frac{-1}{\sqrt{2}}$	0	$\frac{1}{\sqrt{4}}$
3	$\frac{1}{\sqrt{6}}$	0	$\frac{1}{\sqrt{2}}$	0	$\frac{-1}{\sqrt{12}}$	$\frac{1}{\sqrt{4}}$	$\frac{1}{\sqrt{4}}$	0	$\frac{1}{\sqrt{2}}$	$\frac{-1}{\sqrt{4}}$
4	$\frac{1}{\sqrt{6}}$	0	$\frac{-1}{\sqrt{2}}$	0	$\frac{-1}{\sqrt{12}}$	$\frac{1}{\sqrt{4}}$	$\frac{1}{\sqrt{4}}$	0	$\frac{-1}{\sqrt{2}}$	$\frac{-1}{\sqrt{4}}$
5	$\frac{1}{\sqrt{6}}$	0	0	$\frac{1}{\sqrt{2}}$	$\frac{-1}{\sqrt{12}}$	$\frac{-1}{\sqrt{4}}$				
6	$\frac{1}{\sqrt{6}}$	0	0	$\frac{-1}{\sqrt{2}}$	$\frac{-1}{\sqrt{12}}$	$\frac{-1}{\sqrt{4}}$				
Energy	$-4t_{pp}$	0	0	0	$2t_{pp}$	$2t_{pp}$	$-2t_{pp}$	0	0	$2t_{pp}$

combination that is allowed by symmetry to hybridize with the Bi-6s orbital. In the calculated band structures of BaO_3 and O_3, its character is concentrated at the bottom of the O-2p band, mirroring the situation in an isolated octahedron (see the bottom of Table I). As expected, the intensity of the O-a_{1g} character is strongly k-point dependent in the Brillouin zone of a cubic unit cell, vanishing at the Γ point and reaching maximum at the R point. We find little difference between the widths (1.89 eV versus 2.28 eV) and the dispersions of the O-2p bands in the BaO_3 and O_3 sublattices, which indicates that the hybridization between the Ba and O-2p orbitals is much weaker than that between the O-2p orbitals themselves. This is due to a large separation between the O-2p and Ba-5p atomic energy levels as well as a large distance of 3.04 Å between the O and Ba atoms.

We can now appreciate the enormous effect that the Bi-6s–O-2p orbital hybridization has on the electronic structure of $BaBiO_3$, whereby the valence band width increases from 2 eV or less in the isolated sublattices to 15 eV in the full $BaBiO_3$ structure. After the hybridization, the O-a_{1g} molecular orbital in an antibonding combination with the 6s orbital lands above the Fermi level [see Figs. 1(g) or 1(h)]. Such behavior of the O-a_{1g} molecular orbital paves the path for the bipolaronic condensation of oxygen holes upon breathing distortion, as will be discussed later.

Apart from being strongly coupled via $sp\sigma$-type overlap integrals, the hybridizing Bi-6s atomic orbital and the O-a_{1g} molecular orbital also take advantage of their energetic proximity. To demonstrate this, the position of the Bi-6s band in, e.g., the Bi sublattice in Fig. 1(c) has been aligned with that in $BaBiO_3$ at the Γ point where the Bi-6s–O-2p hybridization vanishes by symmetry, marking the Bi-6s on-site energy at ϵ_s=−6.1 eV. Similarly, the top of the O-2p band in the BaO_3 sublattice in Fig. 1(e) has been aligned with the top of the O-2p nonbonding states in $BaBiO_3$. After such alignments, one clearly sees that the Bi-6s orbital is only about 2 eV below the O-a_{1g} molecular orbital which is much smaller than the hopping integral between the O-a_{1g} and the Bi-6s orbitals.

B. Derivation of tight-binding models for BaO_3, O_3, and $BaBiO_3$

In order to quantify the hybridization effects discussed above, we will now derive minimal tight-binding models for $BaBiO_3$ and its BaO_3 and O_3 sublattices by fitting their DFT band structures. In all our nearest-neighbor TB models, there are two intersite oxygen hopping integrals $t_{pp\sigma}$ and $t_{pp\pi}$. We additionally include an $sp\sigma$ hopping integral between the Ba-6s and O-2p orbitals, $t_{sp\sigma}^{\text{Ba-O}}$, for the BaO_3 sublattice and an $sp\sigma$ hopping integral between the Bi-6s and O-2p orbitals, $t_{sp\sigma}$, for $BaBiO_3$. These simple models can nevertheless provide an overall good description of the DFT band structure, see Figs. 1(e)–1(g). The parameter values resulting from the fits are listed in Table II. The Bi-6s–O-2p hybridization parameter $t_{sp\sigma} = 2.10$ eV is indeed found to be by far the dominant hopping integral in the system.

Surprisingly, the ratios $|t_{pp\sigma}|/|t_{pp\pi}| = 5$ in O_3 and $|t_{pp\sigma}|/|t_{pp\pi}| = 10$ in $BaBiO_3$ are considerably larger than the empirical ratio of 3 typically assumed in cuprates [29,30]. The origin of such an enhancement of the $|t_{pp\sigma}|/|t_{pp\pi}|$ ratio is not clear, although we have ruled out a possible sensitivity of this parameter to the system's dimensionality and to the O-O bond length variation by comparing calculations with accordingly modified structural parameters.

For $BaBiO_3$, we also find that the TB model parameter values are in good agreement with hopping integrals calculated using Wannier function (WF) projections [31,32], where we only included Bi-6s and O-2p orbitals, since the low energy states spanning the Fermi energy are primarily of O-2p and Bi-6s character (see the fourth column of Table II). However, this technique gives an unphysically large next-nearest-neighbor hopping between the O-p_σ orbitals $t'_{pp\sigma}$. This result is a

TABLE II. On-site energies and hopping integrals in eV for $BaBiO_3$ and its O_3 and BaO_3 sublattices. The values are obtained by fitting either the simplest or the extended tight-binding (TB or ETB) model or by using Wannier functions (WF) including Bi-6s and O-2p orbitals. This choice of WF orbitals results in a large next-nearest-neighbor hopping integral $t'_{pp\sigma}$ between the O-2p_σ orbitals.

	O_3	BaO_3	$BaBiO_3$		
	TB	TB	TB	WF	ETB
ϵ_s			−4.73	−6.93	−6.2
ϵ_{p_σ}	−2.57	−2.92	−5.13	−4.84	−3.11
ϵ_{p_π}	−2.49	−2.82	−3.06	−3.73	−2.78
$t_{pp\sigma}$	0.26	0.30	0.63	0.64	0.4
$t_{pp\pi}$	−0.05	−0.01	−0.04	−0.03	−0.03
$t_{sp\sigma}$			2.10	2.31	2.09
ϵ_s^{Ba}		3.47			
$t_{sp\sigma}^{\text{Ba-O}}$		0.9			
$t'_{pp\sigma}$				−1.0	
ϵ_p^{Bi}					2.1
$t_{pp\sigma}^{\text{Bi-O}}$					2.34
$t_{pp\pi}^{\text{Bi-O}}$					−0.53

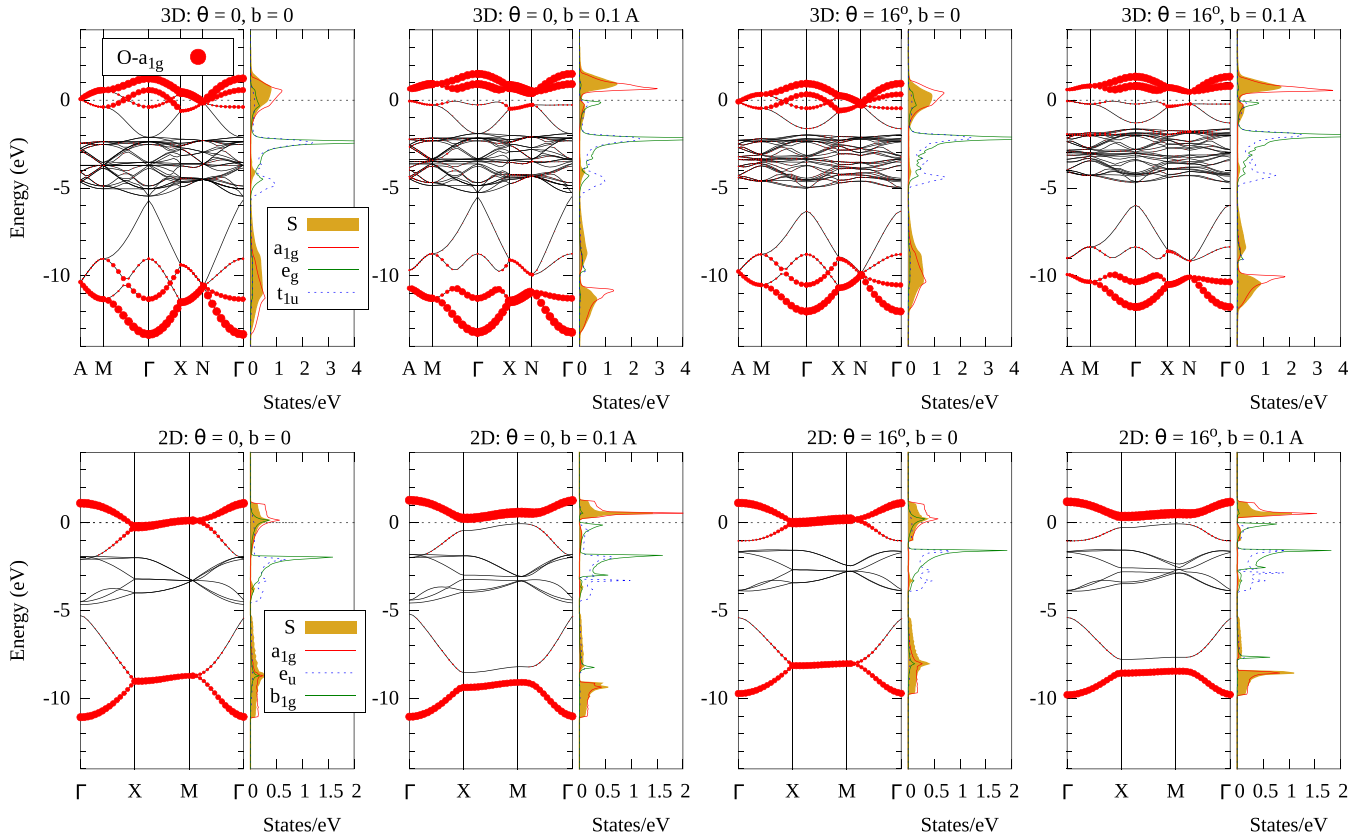

FIG. 2. The band structures and projected DOS of the 3D (top panels) and 2D (bottom panels) TB models with varying strengths of the breathing and tilting distortions. Here, breathing b is half the difference between the two disproportionated Bi-O bond lengths, and θ is the tilting angle. Molecular orbital projections are made for the compressed octahedron or square plaquette following Table I, while the Bi-s orbital projection is made for the Bi atom located inside the compressed octahedron or square plaquette. The red-colored fat bands represent the contribution of the O-a_{1g} molecular orbital.

consequence of the rather strong hybridization of the O-2p orbitals with the empty Bi-6p orbitals, which have not been included in the Wannier basis. It has motivated us to also consider an extended tight-binding (ETB) model with added hybridization between the O-2p and Bi-6p orbitals (see the fifth column of Table II). The ETB model indeed provides an improved description of the DFT band structure [see Fig. 1(h)], but also gives a more realistic value for the Bi-6s orbital on-site energy $\epsilon_s = -6.2$ eV, which is very close to the value of -6.1 eV corresponding to the position of the strongest Bi-6s character band at Γ in Fig. 1(a).

C. Breathing and tilting distortions in two and three dimensions

In this section, we will consider lattice distortions present in the real $ABiO_3$ structure. We are interested in whether our TB model can capture the changes in the electronic structure due to the lattice distortions as observed in DFT calculations [25], such as the opening of the charge gap with the onset of the breathing distortion. Behaviors of the TB model in three and two dimensions will be compared to study the role of dimensionality in the problem.

Since our focus is mainly on the top valence band crossing the Fermi level, which is of the O-a_{1g} symmetry and does not mix with the Bi-6p orbital, we will use here the simpler TB model from the third column of Table II with only Bi-6s and O-2p orbitals in the basis. The coupling of electrons to lattice distortions is modeled through a $1/d^2$ dependence of hopping integrals on the interatomic separation d [29].

In order to study the individual roles of the breathing and tilting distortions, let us consider four model structures of $ABiO_3$ with the following characteristics: (i) $b = 0$ Å, $\theta = 0°$, (ii) $b = 0.1$ Å, $\theta = 0°$, (iii) $b = 0$ Å, $\theta = 16.5°$, and (iv) $b = 0.1$ Å, $\theta = 16.5°$. Here, b is half the difference between the two disproportionated Bi-O bond lengths and θ is the tilting angle of the octahedron in three-dimensions, or the rotation of the square plaquette in two-dimensions. The values of $b = 0.1$ Å and $\theta = 16.5°$ in structure (iv) correspond to the respective strengths of the breathing and tilting distortions in the experimental $SrBiO_3$ structure. Because the distortions break translational symmetry, there are four formula units in the three-dimensional (3D) unit cell and two formula units in the two-dimensional (2D) unit cell.

Figure 2 presents the band structures and the projected densities of states (DOS) of our 3D (top panels) and 2D (bottom panels) model structures. Molecular orbital projections are made for the compressed octahedron or square plaquette following Table I, and the red-colored fat bands represent the contribution of the O-a_{1g} molecular orbital. We find that the models' electronic structure exhibit similar characteristics irrespective of the dimensionality. Close to the Fermi level, the

TABLE III. Variation of the nearest-neighbor hopping integrals in response to the Bi-O bond disproportionation of 0.1 Å.

	$t_{sp\sigma}$ (eV)	$t_{pp\sigma}$ (eV)	$t_{pp\pi}$ (eV)
$b = 0$ Å, $\theta = 0$ °	2.1	0.63	−0.04
$b = 0.1$ Å, $\theta = 0$ °	2.37 1.96	0.71 0.59	−0.045 −0.03

tilting distortion opens a gap at around −1.5 eV and causes an overall band narrowing while the breathing distortion opens a charge gap transforming the system into a semiconductor. This metal-to-semiconductor transition is accompanied by a shift of the O-a_{1g} molecular orbital character into the empty states. Its intensity becomes k-point independent meaning that in real space holes spatially condense into well-defined molecular orbitals on the collapsed octahedra. The observed strong tendency towards formation of molecular orbitals can be due to the fact that oxygen hopping integrals are rather sensitive to the Bi-O bond disproportionation. As one can see in Table III, bond disproportionation of 0.1 Å results in 0.4 eV difference in the $t_{sp\sigma}$ hopping integrals for the collapsed and the expanded octahedron.

Let us also have a closer look at the behavior of the charge gap as a function of t and b. It is depicted in Figs. 3(a) and 3(b) for the 2D and 3D TB models, respectively. In both cases, the gap is linear in b but its θ dependence is stronger in the 2D case. Qualitatively our model calculations can reproduce the DFT results for $SrBiO_3$ [25] [Fig. 3(c)], but quantitatively the effects of both the breathing and tilting distortions are rather underestimated, especially in the 3D case. This is due to the approximations we used in the model calculations, such as neglecting the variation of on-site energies or limiting the number of orbitals. To exemplify the effect of the latter approximation, we compare the DFT gap in $SrBiO_3$ with that

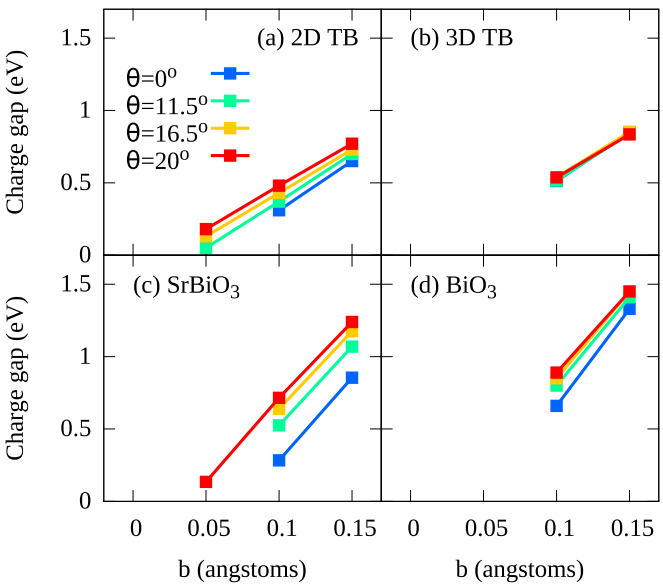

FIG. 3. The charge gap as a function of the breathing distortion at various tilting distortions in (a) the 2D TB model, (b) the 3D TB model, (c) $SrBiO_3$ from DFT (LDA) calculations [25], and (d) the BiO_3 sublattice from DFT (LDA) calculations.

in BiO_3 [Fig. 3(d)]. Here, the θ dependence of the gap is noticeably reduced, similarly to what we find in the model calculations where the A cation orbitals are also neglected. This suggests that hybridization with the A cation orbitals plays a role in defining the size of the charge gap as a function of θ.

D. Tight-binding models with a reduced number of orbitals

Finally, we discuss possible simplifications of the $ABiO_3$ TB model that would still allow an accurate description of low-energy electronic excitations. As was shown previously, the bands straddling the Fermi level are dominantly of the Bi-s and O-p_σ orbital character. Therefore, a natural simplification of the TB model could be to eliminate the O-p_π orbitals from the basis. This reduces the basis size from ten to four orbitals per formula unit. As one can see in Figs. 4(a) and 4(b), the four-orbital TB model gives good agreement with the full ten-orbital model near the Fermi level even without adjustment of model parameters. Here, the calculations are done for a face-centered cubic unit cell with two Bi sites, and the nondistorted lattice [panel (a)] is compared with a lattice featuring an 0.1 Å breathing distortion and no octahedra tilting [panel (b)]. The comparison illustrates, in particular, that the four-orbital model is capable of describing the distortion-induced metal-to-semiconductor transition in $ABiO_3$.

Despite its reduced basis size, the four-orbital model, however, contains redundant degrees of freedom, as far as low-energy physics is concerned. They give rise to the bonding Bi-s and O-p_σ states at −10 eV and the oxygen nonbonding states at −3 eV, i.e., in the energy regions deep below the Fermi level. One can take a step further and write down a single-orbital TB model with an A_{1g}-symmetric orbital at each octahedron site. For this model, which could represent only the low energy scale bands, the basis consists of antibonding combinations of Bi-s and O-a_{1g} orbitals:

$$|\psi^{A_{1g}}\rangle = \frac{1}{\sqrt{\alpha^2+\beta^2}}(\alpha|\psi^{\mathrm{Bi}-s}\rangle - \beta|\psi^{\mathrm{O}-a_{1g}}\rangle),$$

where $\psi^{\mathrm{O}-a_{1g}}$ orbital is a symmetric linear combination of O-p$_\sigma$ [Fig. 1(d)]. Neglecting spin, the effective Hamiltonian in this basis can be written as:

$$H = \sum_i \epsilon^c_{A_{1g}} \hat{c}_i^\dagger \hat{c}_i + \sum_j \epsilon^e_{A_{1g}} \hat{d}_j^\dagger \hat{d}_j + H^{c-e} + H^{c-c} + H^{e-e}.$$

Here, indices i and j run over collapsed and expanded octahedron sites, respectively; $\hat{c}_i^\dagger$ ($\hat{c}_i$) create (annihilate) a hole on site i and $\hat{d}_j^\dagger$ ($\hat{d}_j$) create (annihilate) a hole on site j; $\epsilon^c_{A_{1g}}$ ($\epsilon^e_{A_{1g}}$) is the on-site energy of the A_{1g} orbital on a collapsed (expanded) octahedron site. The hybridization terms can be written as:

$$H^{c-e} = \sum_{<ij>}^{n.n.} t \hat{c}_i^\dagger \hat{d}_j + \mathrm{H.c.}$$

$$H^{c-c} = \sum_i \sum_{i' \in \{i\}} t' \hat{c}_i^\dagger \hat{c}_{i'} + \sum_i \sum_{i'' \in \{i\}} t'' \hat{c}_i^\dagger \hat{c}_{i''} + \mathrm{H.c.}$$

$$H^{e-e} = \sum_j \sum_{j' \in \{j\}} t' \hat{d}_j^\dagger \hat{d}_{j'} + \sum_j \sum_{j'' \in \{j\}} t'' \hat{d}_j^\dagger \hat{d}_{j''} + \mathrm{H.c.},$$

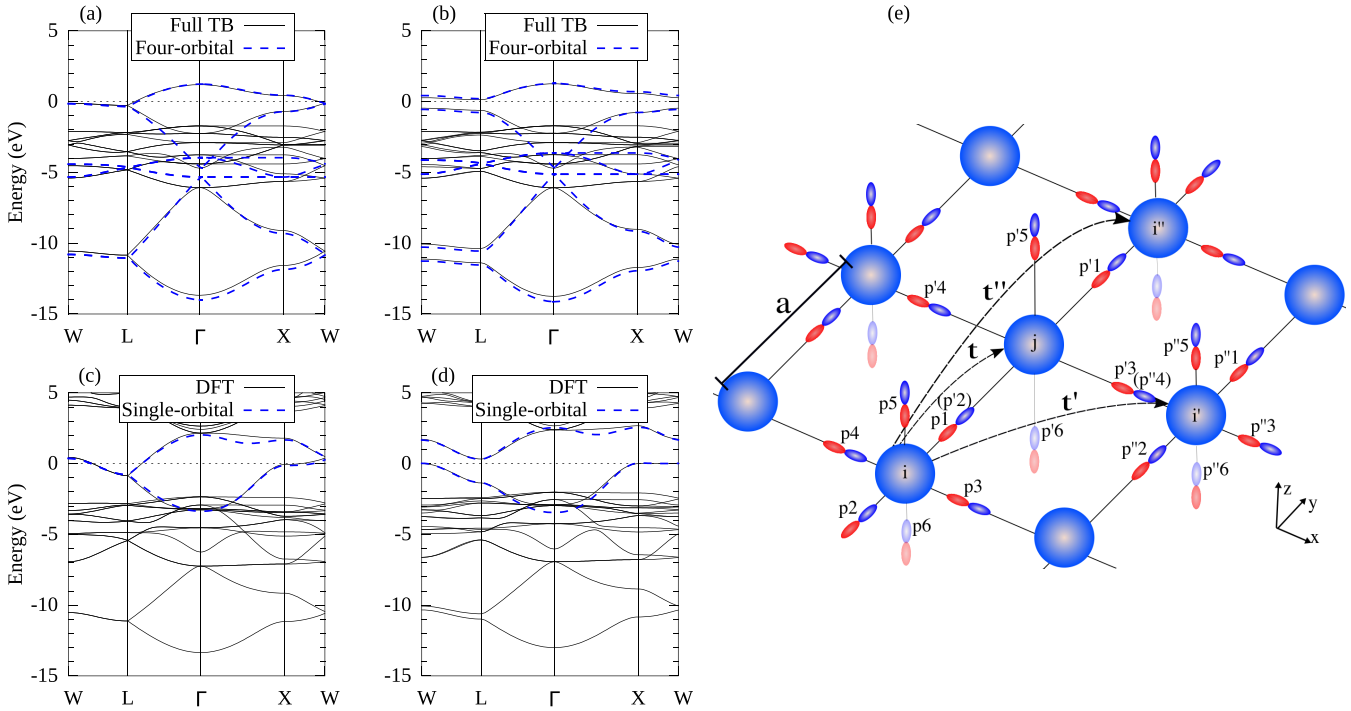

FIG. 4. In (a) and (b), the full TB (solid line) and the four-orbital TB (dashed line) models are compared for the $b = 0.0$ Å and $b = 0.1$ Å lattices, respectively. In (c) and (d), the DFT band structure (solid line) and the single-orbital TB model (dashed line) are compared for the $b = 0.0$ Å and $b = 0.1$ Å lattices, respectively. In (e), the single-orbital A_{1g} coupling to nearest, second nearest, and fourth nearest neighbors are shown.

where $< ij >$ represents sum over nearest-neighbor sites, i' and i'' (j' and j'') are sites at distances $\sqrt{2}a$ and $2a$ from site $i(j)$, respectively [Fig. 4(e)]. The model parameter values are obtained by fitting to the DFT states closest to the Fermi level. The parameter values are given in Table IV for lattices with a varying degree of the breathing distortion, and the fits for the $b = 0$ Å and $b = 0.1$ Å lattices are shown in Figs. 4(c) and 4(d), respectively. We find that within the single-orbital TB model the appearance and growth of the charge gap with an increasing breathing distortion can be well described by a splitting of the two A_{1g} orbital on-site energies, with essentially no need of modifying the hopping integrals [see Table IV]. This model can be interpreted as an effective low energy model of bismuthates that can well describe the bands near the Fermi level and can now be used for example to include electron-phonon coupling keeping in mind the origin of these wave functions and the effects of electron or hole doping looking for possible superconductivity.

In order to clarify the physics involved in these effective hopping integrals, it is instructive to obtain estimates for hopping integrals, t, t', and t'' by considering the composition of the A_{1g} orbitals described above. These hoppings can be directly related to our full ten orbital model parameters, $t_{pp\sigma}$, $t_{pp\pi}$, and $t_{sp\sigma}$, with taking into account O-O and Bi-O hoppings only up to nearest neighbor. In the following, we consider for simplicity a nondistorted case, approximate the coefficients α and β to be $\alpha = \beta = 1$, and also neglect the nonorthogonality that occurs in the O-a_{1g} orbitals on nearest neighbors in estimating t, since the overlap is only $\frac{1}{6}$. The A_{1g} nearest-neighbor hopping t [see Fig. 4(e)] can be written as:

$$t = \langle \psi_i^{A_{1g}} | H | \psi_j^{A_{1g}} \rangle = \left\langle \frac{1}{\sqrt{2}} \left(\psi^s - \frac{1}{\sqrt{6}} (-p_1 + p_2 - p_3 + p_4 - p_5 + p_6) \right)_i \right|$$

$$\times H \left| \frac{1}{\sqrt{2}} \left(\psi^s - \frac{1}{\sqrt{6}} (-p'_1 + p'_2 - p'_3 + p'_4 - p'_5 + p'_6) \right)_j \right\rangle$$

$$= -\frac{1}{2\sqrt{6}} \langle \psi_i^s | H | p'_{2_j} \rangle + \frac{1}{2\sqrt{6}} \langle p_{1_i} | H | \psi_j^s \rangle + \frac{1}{12} \langle -p_{1_i} | H | (-p'_3 + p'_4 - p'_5 + p'_6)_j \rangle + \frac{1}{12} \langle (-p_3 + p_4 - p_5 + p_6)_i | H | p'_{2_j} \rangle$$

$$= -\frac{1}{\sqrt{6}} t_{sp\sigma} + \frac{2}{3} t_{pp} = -\frac{1}{\sqrt{6}} t_{sp\sigma} + \frac{1}{3} (t_{pp\sigma} - t_{pp\pi}) \approx -0.64 \text{ eV}.$$

The next-nearest neighbor hopping term can be written:

$$\begin{aligned} t' &= \langle \psi_i^{A_{1g}} | H | \psi_{i'}^{A_{1g}} \rangle \\ &= \left\langle \frac{1}{\sqrt{2}} \left(\psi^s - \frac{1}{\sqrt{6}}(-p_1 + p_2 - p_3 + p_4 - p_5 + p_6) \right)_i \middle| H \middle| \frac{1}{\sqrt{2}} \left(\psi^s - \frac{1}{\sqrt{6}}(-p_1'' + p_2'' - p_3'' + p_4'' - p_5'' + p_6'') \right)_{i'} \right\rangle \\ &= \frac{1}{2} \times \frac{1}{6} \langle (p_1 + p_3)_i | H | (-p_2'' - p_4'')_{i'} \rangle = -\frac{2}{12} t_{pp} = \frac{1}{12}(-t_{pp\sigma} + t_{pp\pi}) \approx -0.05 \text{ eV}, \end{aligned}$$

and the fourth nearest-neighbor term:

$$\begin{aligned} t'' &= \langle \psi_i^{A_{1g}} | H | \psi_{i''}^{A_{1g}} \rangle = \langle \psi_i^{A_{1g}} | \psi_j^{A_{1g}} \rangle \langle \psi_j^{A_{1g}} | H | \psi_{i''}^{A_{1g}} \rangle = \langle \psi_i^{A_{1g}} | \psi_j^{A_{1g}} \rangle \times t \\ &= \left\langle \frac{1}{\sqrt{2}} \left(\psi^s - \frac{1}{\sqrt{6}}(-p_1 + p_2 - p_3 + p_4 - p_5 + p_6) \right)_i \middle| \frac{1}{\sqrt{2}} \left(\psi^s - \frac{1}{\sqrt{6}}(-p_1' + p_2' - p_3' + p_4' - p_5' + p_6') \right)_j \right\rangle \times t \\ &= \frac{1}{2} \times \frac{1}{6} \langle -p_1 | p_2' \rangle \times t \approx +0.05 \text{ eV}, \end{aligned}$$

where $\langle \psi_i^{A_{1g}} | \psi_j^{A_{1g}} \rangle = -\frac{1}{12}$ is the overlap integral between site i and j. The above estimates are within the order of magnitude of the single-orbital parameters in Table IV obtained from the fit. For the on-site energies we have:

$$\begin{aligned} \epsilon_{A_{1g}} &= \langle \psi_i^{A_{1g}} | H | \psi_i^{A_{1g}} \rangle = \frac{1}{2} \langle (\psi^s - \psi^{a_{1g}})_i | H | (\psi^s - \psi^{a_{1g}})_i \rangle \\ &= \frac{1}{2}(\epsilon_s + \epsilon_{a_{1g}}) - \frac{6}{\sqrt{6}} t_{sp\sigma}, \end{aligned}$$

where on-site energy of O-a_{1g} is $\epsilon_{a_{1g}} = \epsilon_\sigma - 4t_{pp}$ and $\frac{6}{\sqrt{6}} t_{sp\sigma}$ is the coupling energy of Bi-s and O-a_{1g} orbitals. The change in the on-site energies due to breathing can now be written as:

$$\begin{aligned} \Delta\epsilon &= \epsilon_{A_{1g}}^c - \epsilon_{A_{1g}}^e \\ &= \left(-2t_{pp}^c - \frac{6}{\sqrt{6}} t_{sp\sigma}^c \right) - \left(-2t_{pp}^e - \frac{6}{\sqrt{6}} t_{sp\sigma}^e \right). \end{aligned}$$

Here, $t_{pp}^c (t_{pp}^e)$ represent O-O hoppings [see Fig. 1(d)] of the collapsed (expanded) A_{1g} orbitals, and $t_{sp\sigma}^c (t_{sp\sigma}^e)$ are the corresponding Bi-O hoppings, and we have assumed that Bi-s on-site energies are unchanged. Using hopping parameters of a distorted lattice of 0.1 Å from Table III, a direct gap value of $\Delta\epsilon \approx 1.1$ eV is estimated. This value of the gap is comparable to $\Delta\epsilon$ in Table IV obtained from the fit.

TABLE IV. The single-orbital TB model parameter values in eV for lattices with a varying degree of the breathing distortion b and no octahedra tilting. t, t', and t'' are the nearest, second-nearest, and fourth-nearest neighbor hopping integrals, respectively. $\epsilon_{A_{1g}}^c$ and $\epsilon_{A_{1g}}^e$ are the on-site energies of the A_{1g}-like orbitals of the collapsed and expanded octahedron. Bond disproportionation (B.D.) shows the number of A_{1g}^c orbital holes.

b	$\epsilon_{A_{1g}}^c$	$\epsilon_{A_{1g}}^e$	t	t'	t''	B.D.
0.00 Å	−0.13	−0.13	−0.45	−0.09	0.10	1.00
0.05 Å	0.35	−0.51	−0.47	−0.10	0.11	1.46
0.10 Å	0.99	−0.65	−0.48	−0.11	0.115	1.68
0.15 Å	1.86	−0.78	−0.50	−0.12	0.125	1.78

In Table IV we show an effective orbital occupation corresponding to the number of holes in the collapsed A_{1g}^c orbital calculated by integrating the projected density of states above the chemical potential as a function of the breathing distortion. Since we have two Bi and two holes per unit cell the number of holes in the expanded A_{1g}^e orbital is also 1.0 for no breathing. As the distortion increases we see that the number of holes in the collapsed A_{1g}^c molecular orbital gradually moves towards 2.0 at which point there would be no holes anymore in the expanded A_{1g}^e molecular orbital. This looks very much like charge disproportionation. However, in the structure all the oxygens are identical which means that this cannot be charge disproportionation involving the oxygen. Each oxygen indeed participates in both the collapsed and expanded A_{1g} molecular orbitals however it participates more in the collapsed A_{1g}^c molecular orbital than in the expanded one. So again, this has to do with bond disproportionation. We note however that there is no symmetry change in moving from a bond to a charge-disproportionation picture and so there is no clear boundary but rather a gradual crossover. A real charge disproportionation would have to imply an attractive coulomb interaction while a bond disproportionation results from the electron density changes in the bonds driven by an electron-phonon coupling involving the hopping integral changes.

We can infer the electron-phonon coupling strength from our single-orbital model as the A_{1g} molecular orbital on-site energy lowering in Table IV, which is about 1 eV in the presence of the experimental bond modulation of 0.1 Å or equivalently $\frac{d\epsilon}{dx} = 10$ eV/Å. Given a Raman breathing mode phonon frequency of $\omega_{\text{ph}} \approx 70$ meV [33,34] at $q = (\pi,\pi,\pi)$ for $BaBiO_3$ the electron-phonon coupling g can be estimated as:

$$g = \frac{\partial\epsilon}{\partial x} \sqrt{\frac{\hbar}{2M_o\omega_{\text{ph}}}} \approx 10 \text{ eV/Å} \times 0.04321 \text{ Å} \approx 0.4321 \text{ eV},$$

where M_o is the oxygen mass. The electron-phonon coupling g translated into the dimensionless coupling λ is:

$$\lambda = \frac{2g^2}{\hbar\omega_{\text{ph}} W} = \frac{2 \times 0.4321^2}{0.07 \times 6} \approx 0.89,$$

where $W \approx 6$ eV is the single-orbital A_{1g} bandwidth read from Fig. 4(d). Following the same argument we can estimate a value of $\lambda = 1.21$ for $Ba_{0.6}K_{0.4}BiO_3$ given a breathing mode phonon frequency of $\omega_{ph} \approx 60$ meV [35] for $Ba_{0.6}K_{0.4}BiO_3$ and assuming that the bandwidth W is unchanged upon K substitution. These electron-phonon couplings are much higher than what has been obtained from previous LDA calculations on $Ba_{0.6}K_{0.4}BiO_3$ [36–41]. Of course, to make a real comparison with LDA estimates one would have to determine the q dependence of this coupling and average this over an assumed Fermi surface.

III. CONCLUSIONS

In summary, we have studied the electronic structure of the bismuth perovskites $ABiO_3$ (A = Sr, Ba) using *ab initio* calculations and tight-binding modeling. We found that the hopping integrals involving the Bi-6s and O-2p orbitals play a leading role in shaping the electronic band structure of $ABiO_3$ near the Fermi level. A minimal TB model with ten orbitals per formula unit (one Bi-6s and nine O-2p orbitals) was derived and shown to be able to describe the changes in the electronic structure due to lattice distortions that had been observed in previous DFT studies, such as the opening of the charge gap due to the breathing distortion and the associated formation of molecular orbitals on collapsed octahedra. We also showed that for the purpose of exploring low-energy excitations in $ABiO_3$ this TB model can be further reduced to a four-orbital one with one Bi-6s and three O-2p_σ orbitals in the basis and even further down to a single-orbital one with a single A_{1g}-like orbital at each octahedron site. Within this model, we further estimated electron-phonon couplings of $\lambda = 0.89$ and $\lambda = 1.21$ for $BaBiO_3$ and $Ba_{0.6}K_{0.4}BiO_3$ respectively. This single band model is a good representation of the band structure close to the chemical potential and can be used in a more detailed study including the influence of electron-phonon coupling and possible mechanisms for superconductivity in the doped materials, but one has to keep in mind the rather extended molecular orbital character of the basis states in such a model.

ACKNOWLEDGMENTS

This work was supported by Natural Sciences and Engineering Research Council (NSERC) for Canada, Canadian Institute for Advanced Research (CIFAR), and the Max Planck-UBC Stewart Blusson Quantum Matter Institute.

[1] R. J. Cava, B. Batlogg, J. J. Krajewski, R. Farrow, L. W. R. Jr., A. E. White, K. Short, W. F. Peck, and T. Kometani, Nature (London) **332**, 814 (1988).
[2] A. Sleight, J. Gillson, and P. Bierstedt, Solid State Commun. **17**, 27 (1975).
[3] S. M. Kazakov, C. Chaillout, P. Bordet, J. J. Capponi, M. Nunez-Regueiro, A. Rysak, J. L. Tholence, P. G. Radaelli, S. N. Putilin, and E. V. Antipov, Nature (London) **390**, 148 (1997).
[4] D. Cox and A. W. Sleight, Solid State Commun. **19**, 969 (1976).
[5] D. E. Cox and A. W. Sleight, Acta Crystallogr. Sect. B **35**, 1 (1979).
[6] A. M. Glazer, Acta Crystallogr. Sect. B **28**, 3384 (1972).
[7] A. M. Glazer, Acta Crystallogr. Sect. A **31**, 756 (1975).
[8] C. M. Varma, Phys. Rev. Lett. **61**, 2713 (1988).
[9] I. Hase and T. Yanagisawa, Phys. Rev. B **76**, 174103 (2007).
[10] W. A. Harrison, Phys. Rev. B **74**, 245128 (2006).
[11] G. Vielsack and W. Weber, Phys. Rev. B **54**, 6614 (1996).
[12] L. F. Mattheiss and D. R. Hamann, Phys. Rev. B **28**, 4227 (1983).
[13] J. de Hair and G. Blasse, Solid State Commun. **12**, 727 (1973).
[14] A. F. Orchard and G. Thornton, J. Chem. Soc., Dalton Trans. 1238 (1977).
[15] G. K. Wertheim, J. P. Remeika, and D. N. E. Buchanan, Phys. Rev. B **26**, 2120 (1982).
[16] N. C. Plumb, D. J. Gawryluk, Y. Wang, Z. Ristic, J. Park, B. Q. Lv, Z. Wang, C. E. Matt, N. Xu, T. Shang, K. Conder, J. Mesot, S. Johnston, M. Shi, and M. Radovic, Phys. Rev. Lett. **117**, 037002 (2016).
[17] C. Franchini, G. Kresse, and R. Podloucky, Phys. Rev. Lett. **102**, 256402 (2009).
[18] C. Franchini, A. Sanna, M. Marsman, and G. Kresse, Phys. Rev. B **81**, 085213 (2010).
[19] D. Korotin, V. Kukolev, A. V. Kozhevnikov, D. Novoselov, and V. I. Anisimov, J. Phys.: Condens. Matter **24**, 415603 (2012).
[20] R. Nourafkan, F. Marsiglio, and G. Kotliar, Phys. Rev. Lett. **109**, 017001 (2012).
[21] Z. P. Yin, A. Kutepov, and G. Kotliar, Phys. Rev. X **3**, 021011 (2013).
[22] D. M. Korotin, D. Novoselov, and V. I. Anisimov, J. Phys.: Condens. Matter **26**, 195602 (2014).
[23] L. F. Mattheiss, Phys. Rev. B **28**, 6629 (1983).
[24] L. F. Mattheiss and D. R. Hamann, Phys. Rev. B **26**, 2686 (1982).
[25] K. Foyevtsova, A. Khazraie, I. Elfimov, and G. A. Sawatzky, Phys. Rev. B **91**, 121114(R) (2015).
[26] A. Ignatov, Nucl. Instrum. Methods Phys. Res., Sect. A **448**, 332 (2000).
[27] P. Blaha, K. Schwarz, G. K. H. Madsen, D. Kvasnicka, and J. Luitz, *WIEN2K, An Augmented Plane Wave + Local Orbitals Program for Calculating Crystal Properties* (Karlheinz Schwarz, Techn. Universitat Wien, Austria, 2001).
[28] J. P. Perdew, K. Burke, and Y. Wang, Phys. Rev. B **54**, 16533 (1996).
[29] S. Froyen and W. A. Harrison, Phys. Rev. B **20**, 2420 (1979).
[30] A. K. McMahan, R. M. Martin, and S. Satpathy, Phys. Rev. B **38**, 6650 (1988).
[31] A. A. Mostofi, J. R. Yates, Y.-S. Lee, I. Souza, D. Vanderbilt, and N. Marzari, Comput. Phys. Commun. **178**, 685 (2008).
[32] J. Kunes, R. Arita, P. Wissgott, A. Toschi, H. Ikeda, and K. Held, Comput. Phys. Commun. **181**, 1888 (2010).
[33] S. Sugai, S. Uchida, K. Kitazawa, S. Tanaka, and A. Katsui, Phys. Rev. Lett. **55**, 426 (1985).
[34] S. Tajima, M. Yoshida, N. Koshizuka, H. Sato, and S. Uchida, Phys. Rev. B **46**, 1232 (1992).

[35] M. Braden, W. Reichardt, A. S. Ivanov, and A. Yu. Rumiantsev, Europhys. Lett. B **34**, 531 (1996).
[36] N. Hamada, S. Massidda, A. J. Freeman, and J. Redinger, Phys. Rev. B **40**, 4442 (1989).
[37] M. Shirai, N. Suzuki, and K. Motizuki, J. Phys.: Condens. Matter **2**, 3553 (1990).
[38] A. I. Liechtenstein, I. I. Mazin, C. O. Rodriguez, O. Jepsen, O. K. Andersen, and M. Methfessel, Phys. Rev. B **44**, 5388 (1991).
[39] K. Kunc and R. Zeyher, Phys. Rev. B **49**, 12216 (1994).
[40] V. Meregalli and S. Y. Savrasov, Phys. Rev. B **57**, 14453 (1998).
[41] T. Bazhirov, S. Coh, S. G. Louie, and M. L. Cohen, Phys. Rev. B **88**, 224509 (2013).